Article

Function of eEF-1γ in the nucleus in response to insulin in hepatocellular carcinoma cells

Check for updates

Abu Jubayer Hossain [1,6], Amir Hamza [1,2,6], Rokibul Islam[1,2,3], Oyungerel Dogsom [1,2,4] & Jae-Bong Park [1,2,5] ✉

Insulin promotes HepG2 cell proliferation by inducing phosphorylation of the pyruvate dehydrogenase E1α (PDHA1) subunit at Ser293, a mechanism distinct from normal liver tissue. This study investigates how phosphorylated PDHA1 drives hepatocellular carcinoma cell proliferation. We identified eukaryotic elongation factor-1γ (eEF-1γ) as a key binding protein interacting with p-PDHA1 in response to insulin, facilitating their nuclear translocation. Silencing eEF-1γ (si-eEF-1γ) significantly reduced p-PDHA1 and PKM2 levels, highlighting eEF-1γ's role in stabilizing these proteins. Additionally, eEF-1γ interacts with ATP-citrate lyase (ACL) and p300 acetyltransferase, and its knockdown decreased histone acetylation at H3K9/14, H3K18, and H3K27, along with RBP4 expression. Chromatin immunoprecipitation PCR (ChIP-PCR) confirmed eEF-1γ association with RBP4 promoter. Functionally, si-eEF-1γ reduced cell proliferation and deceased c-Myc and cyclin D1 protein levels. It also suppressed migration, and altered epithelial-mesenchymal transition (EMT) markers, increasing E-cadherin while reducing ZEB1, snail1, vimentin, and N-cadherin levels. Similarly, RBP4 knockdown with siRNA diminished cell proliferation and migration. In vivo, eEF-1γ knockdown in 4T1 xenografts using siRNA led to reduced tumor mass. These findings highlight eEF-1γ as a crucial driver of insulin-induced tumor progression and suggest its potential as a therapeutic target in hepatocellular carcinoma.

Insulin has multiple functions, one of which is the stimulation of glucose uptake. This leads to glycogen syntheses and the stimulation of lipid synthesis from acetyl-CoA produced from pyruvate by PDH in the liver[1]. Regulation of glucose metabolism plays a crucial role in insulin signaling. Following glycolysis, the tricarboxylic acid (TCA) cycle in mitochondria is initiated by the translocation of pyruvate translocated from cytosol. This process results in the production of various metabolites and ATP. The first critical step in this pathway involves the oxidation of pyruvate, O_2, plus NAD^+ to acetyl-CoA, CO_2, plus $NADH + H^+$ by the pyruvate dehydrogenase (PDH) complex (PDC). The PDC is comprised of PDHE1, dihydrolipoyl transacetylase E2 and dihydrolipoyl dehydrogenase E3 subunits[2]. The activity of PDC enzyme is primarily regulated by phosphorylation at Ser264 (in human, corresponding to Ser293 in mouse) of its PDH E1α (PDHA1) subunit (p-Ser264 PDHA1). Phosphorylation at this

site renders the PDHA1 subunit inactive. The phosphorylation state of PDHA1 is determined by the activities of PDH kinase (PDHK) and PDH phosphatase (PDP)[3]. Insulin, in particular, induces the dephosphorylation of PDHA1 in normal hepatocyte. However, in HepG2 hepatocellular carcinoma, insulin phosphorylates PDHA1 at Ser293, suggesting that insulin enhances PDH activity in normal hepatocytes while decreasing it in hepatocellular carcinoma. This phenomenon is associated with the Warburg effect[4].

Pyruvate kinase (PK) has been well known glycolytic enzyme that catalyzes the final step in converting phosphoenol pyruvate (PEP) plus ADP to pyruvate plus ATP. Pyruvate kinase M1 and M2 (PKM1 and PKM2) are isoforms expressed through alternative splicing of PKM1/2 gene. Specifically, PKM2 is highly expressed in rapidly proliferating cells like embryos and cancer, while PKM1 is only expressed in normal matured cells[5].

[1]Department of Biochemistry, Hallym University College of Medicine, Chuncheon, Kangwon-do, Republic of Korea. [2]Institute of Cell Differentiation and Aging, Hallym University College of Medicine, Chuncheon, Kangwon-do, Republic of Korea. [3]Department of Biotechnology and Genetic Engineering, Faculty of Biological Science, Islamic Uninversity, Kushtia, Bangladesh. [4]Department of Biology, School of Bio-Medicine, Mongolian National University of Medical Sciences, Ulaanbaatar, Mongolia. [5]ELMED Co., Hallym University College of Medicine, Chuncheon, Kangwon-do, Republic of Korea. [6]These authors contributed equally: Abu Jubayer Hossain, Amir Hamza. ✉e-mail: jbpark@hallym.ac.kr

Notably, PKM2 exerts non-metabolic functions in cancers, in addition to its glycolytic function[6]. In detail, PKM2 functions as a transcription factor[7] regulating the expression of specific genes such as glucose transporter 1 (GLUT1), lactate dehydrogenase A (LDHA), and cyclin D1[8,9]. Notably, PKM2 also functions as a protein kinase, phosphorylating histone 3 (H3) at Thr11 residue. This phosphorylation event leads to the expression of cyclin D1 and c-Myc, contributing to tumour cell proliferation[10]. Furthermore, PKM2 phosphorylates Stat3 at Tyr705 as one of its targets[11].

The process of protein synthesis comprises three main steps: initiation, elongation and termination. Eukaryotic elongation factors (eEFs), such as eEF1A and eEF1B, play crucial roles in the elongation step. eEF1A, also known as eEF1α, is responsible for delivering aminoacyl-tRNA to the ribosome. On the other hand, eEF1Bα, also known as eEF1β, acts as a guanine nucleotide exchange factor (GEF) that facilitates the exchange GDP with GTP in eEF1A[12]. Insulin-induced phosphorylation of eEF1 enhances its elongation activity, and this phosphorylation is mediated by S6 kinase[13]. While eEF1γ (eEF1Bγ) is not vital for viability, it serves as a structural scaffold for eEF1Bα (eEF1β). Interestingly, the N-terminal domain of eEF1γ exhibits structural similarity to glutathione S-transferase θ (GSTθ)[14]. Additionally, eEF1γ has been observed to interact with various proteins, including RNA-dependent RNA polymerase of a virus[15] and RNA polymerase II, suggesting its non-conventional functionalities[16].

Recent studies have revealed that in HepG2 cells, p-PDHA1 and PKM2 forms a complex and both localized to the nucleus in response to insulin. This p-PDHA1/PKM2 complex has been shown to regulate the expression of long intergenic non-protein coding RNA 00273 (LINC00273)[17]. Furthermore, our present study has discovered that eEF1γ interacts with p-PDHA1 and PKM2, results in the formation of a trimeric complex that is also localized in the nucleus in response to insulin. We aimed to elucidate the specific role of EF1γ in conjunction with p-PDHA1/PKM2 under insulin stimulation in hepatocellular carcinoma HepG2 cells.

Results

p-Ser293 PDHA1 binds to eEF-1γ

Since p-PDHA1 has been shown to localize in the nucleus, we sought to identify its novel function in this compartment in response to insulin. To achieve this, we prepared the recombinant GST-PDHA1 S293D mutant, a phosphomimic form, conjugated to the bead as bait to capture specific binding proteins. The binding protein was analyzed by MALDI-TOF (Supplementary Fig. S1). We discovered that eukaryotic elongation factor-1γ (eEF-1γ) associated with PDHA1 S293D, phospho-Ser293 PDHA1 mimetic, regardless of insulin stimulation (Fig. 1A). Furthermore, we observed the association of EF-1γ in cell lysates with GST-PDHA1 S293D, but not with GST-PDHA1 WT or GST-PDHA1 S293A, a dephosphomimic form, in vitro (Fig. 1B). Subsequently, we demonstrated the co-immunoprecipitation of p-Ser293 PDHA1 with eEF-1γ (Fig. 1C), and the co-immunoprecipitation of eEF-1γ with p-Ser293 PDHA1 in HepG2 and Huh7 cells (Fig. 1D, E, respectively). In contrast, non-phosphorylated PDHA1 showed minimal co-immunoprecipitation with eEF-1γ (Fig. 1F). Furthermore, we investigated the localization of eEF-1γ, and discovered that eEF-1γ localized in the cytosol in the absence of insulin stimulation. However, in response to insulin treatment, eEF-1γ was observed in the nucleus (Fig. 1G, H). Lastly, we examined the expression levels of eEF-1γ in various cell lines. We found relatively high levels of it in HepG2 cells. Additionally, insulin treatment resulted in elevated levels in several other cell lines, including Huh7, DU-145, 4T1, LN-18, Hepa-1c1c7, MCF-7, and HepG2cells (Fig. 1I).

Insulin induces a trimeric complex of eEF-1γ/p-Ser293 PDHA1/PKM2

We conducted a detailed investigation into the complex formation involving eEF-1γ, p-Ser293 PDHA1 and PKM2 in response to insulin. Our results clearly showed that eEF-1γ co-immunoprecipitated with p-PDHA1 and PKM2 but had minimal interaction with non-phosphorylated PDHA1, as well as PDHE2, and PDHE3 subunits (Fig. 2A). Similarly, PKM2 was observed to co-immunoprecipitate with eEF-1γ and p-PDHA1 in response to insulin treatment (Fig. 2B). We also observed that when eEF-1γ was knocked down using siRNA, the levels of p-PDHA1 and PKM2 were down-regulated. As a result, the co-immunoprecipitation of eEF-1γ with p-PDHA1 and PKM2 were significantly reduced (Fig. 2C). These findings strongly suggest that eEF-1γ plays a crucial role in maintaining the stability of both p-PDHA1 and PKM2. In our in vitro experiments, we found that eEF-1γ binds to the C-terminal domain (CTD) in the absence of insulin, and to the A2 domain and CTD of PKM2 upon insulin stimulation (Fig. 2D). Additionally, PKM2 mainly associated with N-terminal domain (NT), while p-PDHA1 associated with CTD of eEF-1γ (Fig. 2E). When we applied the amine-to-amine cross-linking reagent BS3 [bis(sulfosuccinimidyl)suberate] to the insulin-treated cell lysate, we observed that protein bands of approximately 140 and 200 kDa, in addition to their respective bands of approximately 40–60 kDa. Based on this, we hypothesized that insulin induces a trimeric complex of p-PDHA1, eEF-1γ, and PKM2, with a combined molecular weight of approximately 140 kDa. We presented a simplified diagram of this trimeric complex in Fig. 2F. Furthermore, we observed that p-PDHA1 co-immunoprecipitated with both eEF-1γ and PKM2 in cells transfected with PDHA1 WT and S293D phosphomimetic. However, PDHA1 S293A dephosphomimetic significantly reduced the levels of eEF-1 and PKM2, resulting in rare co-immunoprecipitation with eEF-1γ and PKM2 (Fig. 2G). These findings suggest that the phosphorylation of PDHA1 at Ser293 is crucial for its binding to both eEF-1γ and PKM2. Furthermore, we hypothesized that p-Ser293 PDHA1 may contribute the stability of PKM2 and eEF-1γ. Meanwhile, PKM2 was previously reported to be acetylated at Lys(K)305[18]. We found that PKM2 K305Q, an acetylated mimetic, significantly attenuated co-immunoprecipitation of p-PDHA1 with both PKM2 and eEF-1γ. On the other hand, K305R, a deacetyl-mimetic, did not influence their co-immunoprecipitation (Fig. 2H). This suggests that PKM2 acetylation may impair its interaction with p-PDHA1 and eEF-1γ (Fig. 2H). Moreover, we noticed that eEF-1γ failed to co-immunoprecipitate with p-Tyr105 PKM2, and insulin stimulation reduced the levels of p-Tyr105 PKM2. This indicates that p-Tyr105 of PKM2 is not necessary for the formation of the trimeric complex (Fig. 2I). Additionally, we observed that LPS, another type of stimulants, also promoted the co-immunoprecipitation of PKM2 with p-PDHA1 and eEF-1γ in 4T1 mouse breast cancer cell line (Fig. 2J). This finding suggests that the formation of the trimeric complex involving p-Ser293 PDHA1, PKM2 and eEF-1γ may not be limited to the HepG2/insulin scenario.

eEF-1γ is involved in histone acetylation in the nucleus

Based on the observation that insulin induces histone acetylation in HepG2 cells[17], we aimed to investigate whether eEF-1γ also contributes to the regulation of histone acetylation. As a preliminary experiment, we demonstrated that insulin promoted the acetylation of H3 and H4, and the levels of ACL (Fig. 3A, B, respectively). As we observed the co-immunoprecipitation of p-Tyr42 RhoA with PKM2 in glioma cells[19] and that of p-Tyr42 RhoA with ATP citrate lyase (ACL) in hippocampal cell lines stimulated amyloid-β[20], we explored whether p-Tyr42 RhoA interacts with p-PDHA1 in HepG2 cells in response to insulin. P-Tyr42 RhoA was found to co-immunoprecipitate with both PKM2 and ACL, but with neither p-PDHA1 nor eEF-1γ, irrespective of insulin stimulation (Fig. 3C). Notably, we observed that insulin promoted the co-immunoprecipitation of ACL with PKM2, eEF-1γ, and p-Tyr42 RhoA (Fig. 3D). Moreover, insulin increased the levels of co-immunoprecipitation of p300 acetyltransferase with p-PDHA1, PKM2, and eEF-1γ (Fig. 3E). It is remarkable that knockdown of eEF-1γ using siRNA significantly reduced Ac-H3K27 levels and had a slight effect on the levels of Ac-H3K9/14 and Ac-H3K18 (Fig. 3F). As expected, knockdown of ACL using siRNA significantly abolished the acetylation of H3K9/14, H3K18 and H3K27, indicating that ACL plays a crucial role in providing acetyl-CoA for histone acetylation (Fig. 3G). Consequently, we hypothesized that ACL and PKM2 could collaborate to provide acetyl-CoA for histone acetylation in the nucleus. Furthermore, we found that
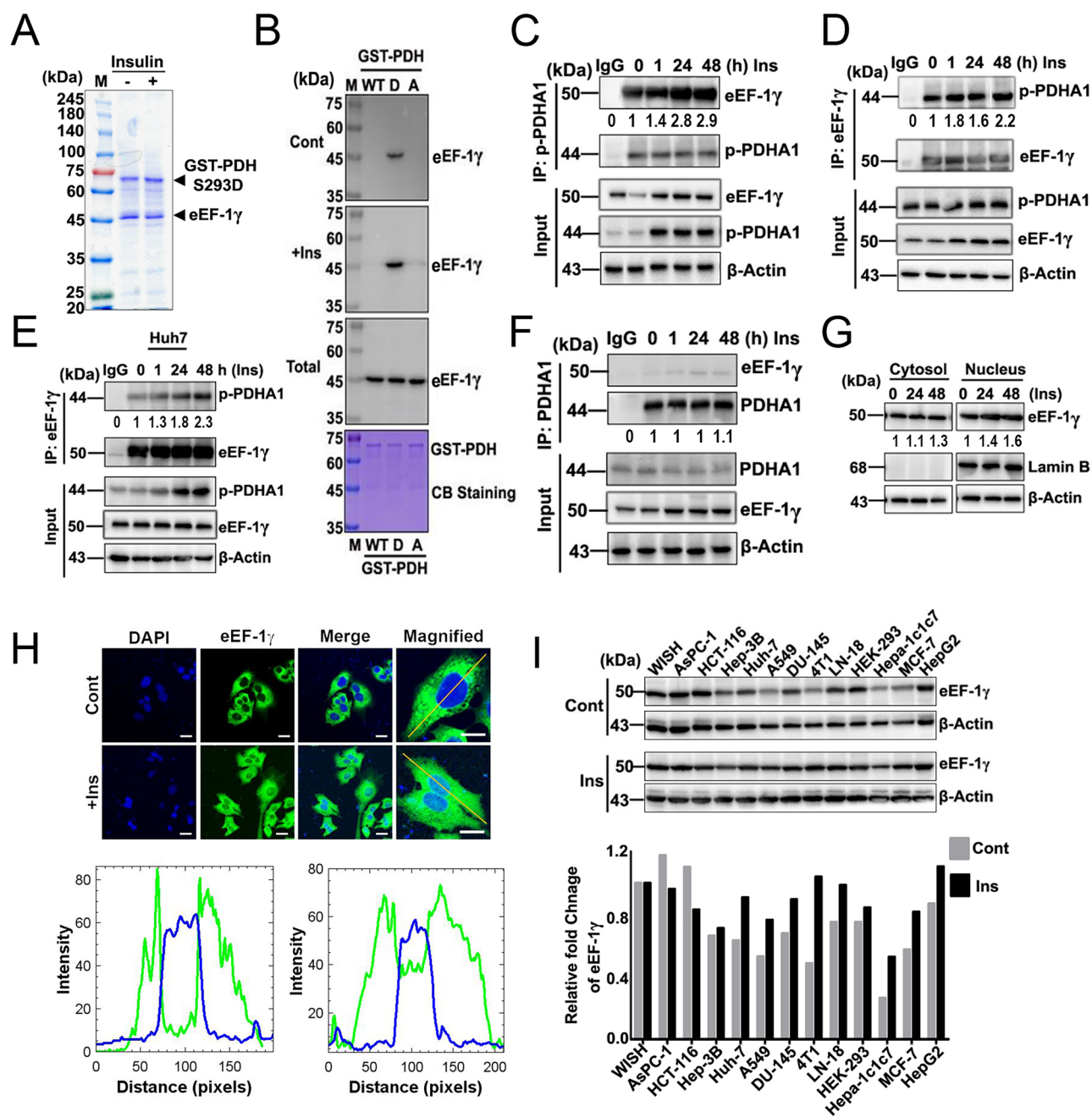
Fig. 1 | eEF-1γ interacts with p-Ser293 PDHA1 and PKM2 upon insulin stimulation. A Nuclear extracts from insulin-treated HepG2 cells were incubated with recombinant GST-PDHA1 S293D, and binding proteins were visualizing by SDS-PAGE and identified via MALDI-TOF analysis, confirming eEF-1γ interaction with p-PDHA1. **B** Western blot analysis of eEF-1γ bound to GST-PDHA1 S293D after incubation with 48 h insulin-treated HepG2 cell lysates. **C–F** Co-immunoprecipitation was performed to analyze the interactions of the p-PDHA1 (**C**), eEF-1γ (**D**) in HepG2 cells, eEF-1γ (**E**) in Huh7 cells, and PDHA1 (**F**) in HepG2 cells respectively, followed by western blot detection of associated proteins. **G** Cytosolic and nuclear fractionation assay were performed and showed eEF-1γ localization along with Lamin B as a nuclear marker detected by western blotting. **H** HepG2 cells were treated with or without insulin and the localization of eEF-1γ (green) was analyzed by confocal microscopy (upper panel). Nuclei are stained blue. Intensity was measured using ImageJ software (bottom panel). **I** Western blot analysis was performed (upper panel) to measure the relative expression levels (bottom panel) of eEF-1γ in different cancer cell lines, with or without insulin treatment. # In each cell-based experiment, 100 nM insulin was used for the indicated time as the stimulated group, while the control group remained untreated. Scale bar (-): 10 μm. Western blot and confocal data are representative of at least three (*n* = 3) independent experiments.

eEF-1γ co-immunoprecipitated with transcription factors, including STAT3 and Oct4, in addition to ACL and p300 (Fig. 3H). Conversely, we detected co-immunoprecipitation of transcription factors such as STAT3, HIF-1α, and Oct4 with p-PDHA1, PKM2 and eEF-1γ, indicating that the trimeric complex of p-PDHA1, PKM2 and eEF-1γ could bind with transcription factors such as STAT3, HIF-1α, and Oct4 (Fig. 3I–K, respectively). These results suggest that eEF-1γ, along with p-PDHA1 and PKM2, along with various transcription factors and the change of histone acetylation is involved in the transcriptional regulation of specific genes.

eEF-1γ regulates the expression of retinoic acid binding protein 4 (RBP4)
Recent epidemiological and clinical evidence demonstrated the association between insulin resistance with hyperinsulinemia and cancer[21].
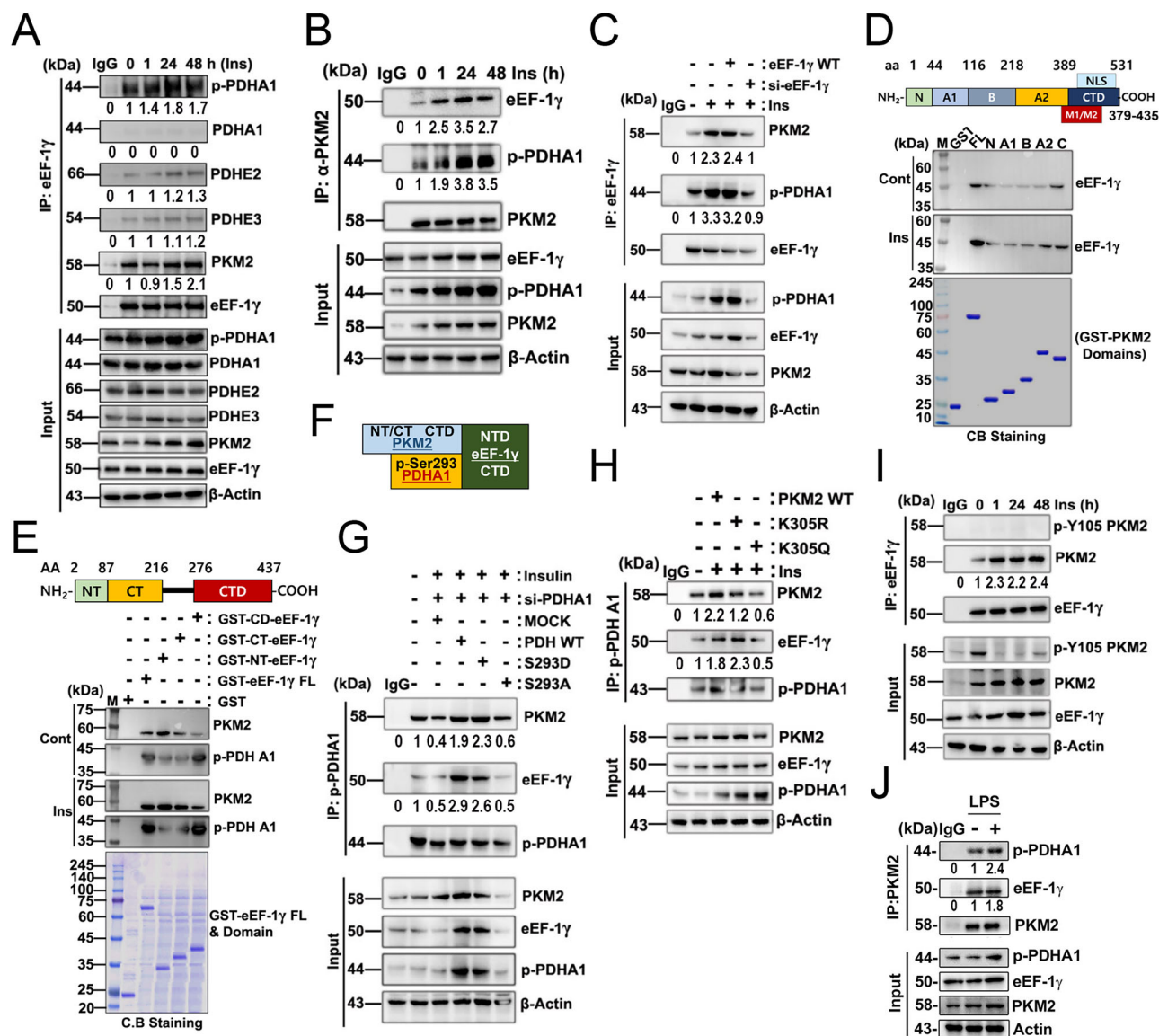
Fig. 2 | Trimeric complex formation among eEF-1γ, p-Ser293 PDHA1, and PKM2. A, **B** Co-immunoprecipitation of eEF-1γ (**A**) and PKM2 (**B**) confirmed their interactions with p-PDHA1 and PKM2 in insulin-stimulated HepG2 cells. **C** HepG2 cells were transfected with si-eEF-1γ and reconstituted with eEF-1γ WT, followed by 100 nM insulin treatment for 24 h. Co-immunoprecipitation was performed using an eEF-1γ antibody, and showed its role in p-PDHA1 and PKM2 binding which were detected by western blotting. **D**, **E** GST-tagged PKM2 (**D**) and eEF-1γ (**E**) recombinant proteins, with their domains conjugated with beads, were incubated with HepG2 cell lysates (stimulated with or without 100 nM insulin for 48 h). Bound proteins were detected by western blotting (upper panel), and protein domains were visualized by Coomassie blue staining (lower panel). **F** Schematic representation of trimeric complex formation. **G**–**J** Co-immunoprecipitation were performed using several antibodies and their target bound proteins were detected by western blotting. **G** PDHA1 knockdown and reconstitution with WT, 293D, and 293 A mutants revealed their effect on complex formation with p-PDHA1. **H** PKM2 acetylation mutants (K305Q, K305R) were analyzed for interaction with p-PDHA1. **I** Co-immunoprecipitation of eEF-1γ confirmed binding with PKM2 and p-Tyr105 PKM2, respectively in HepG2 cells treated with insulin (100 nM) as indicated time periods. **J** LPS (10 µg) stimulated mouse breast cancer 4T1 cells for 4 h was analyzed for PKM2-associated proteins. Western blot data are representative of at least three (n = 3) independent experiments.

Additionally, the elevated levels of RBP4, which is secreted from liver to serum, was found to associate with insulin resistance[22–24]. Notably, RBP4 was observed to associate with the increased risk factor in cancer[25–27]. Based on these documents, we hypothesized that insulin may stimulate cancer progression through RBP4 expression, and that RBP4 expression may be regulated through eEF-1γ in addition to p-PDHA1 and PKM2.

We observed that insulin treatment led to augmentation of RBP4 protein levels in HepG2 and Huh7 cells in a time-dependent manner (Fig. 4A, B, respectively). Similarly, insulin increased in RBP4 mRNA levels in a time-dependent manner (Fig. 4C, D). Notably, si-eEF-1γ suppressed the expression of RBP4 (Fig. 4E), and reconstituted eEF-1γ restored RBP4 expression in cells with si-eEF-1γ-mediated reduced RBP4

expression (Fig. 4F), suggesting that eEF-1γ is crucial for the RBP4 expression. Additionally, we found that si-PDHA1 and si-PKM2 as well as si-eEF-1γ abolished RBP4 expression (Fig. 4G). Interestingly si-eEF-1γ suppressed PKM2 and p-PDHA1, but not PDHA1. Si-PDHA1 suppressed eEF-1γ and PKM2, while si-PKM2 suppressed eEF-1γ and p-PDHA1, but not PDHA1 (Fig. 4G). These results suggest that the trimeric complex is necessary for their stability. Moreover, we found that reconstitution of PDHA1 WT and PDHA1 S293D, but not S293A rescued RBP4 expression in si-PDHA1-transfected HepG2 cells, suggesting that Ser293 phosphorylation in PDHA1 is essential for RBP4 expression (Fig. 4H). It was remarkable to find that p-PDHA1, PKM2 and eEF-1γ associate with RBP4 promoter through ChIP-PCR experiments using
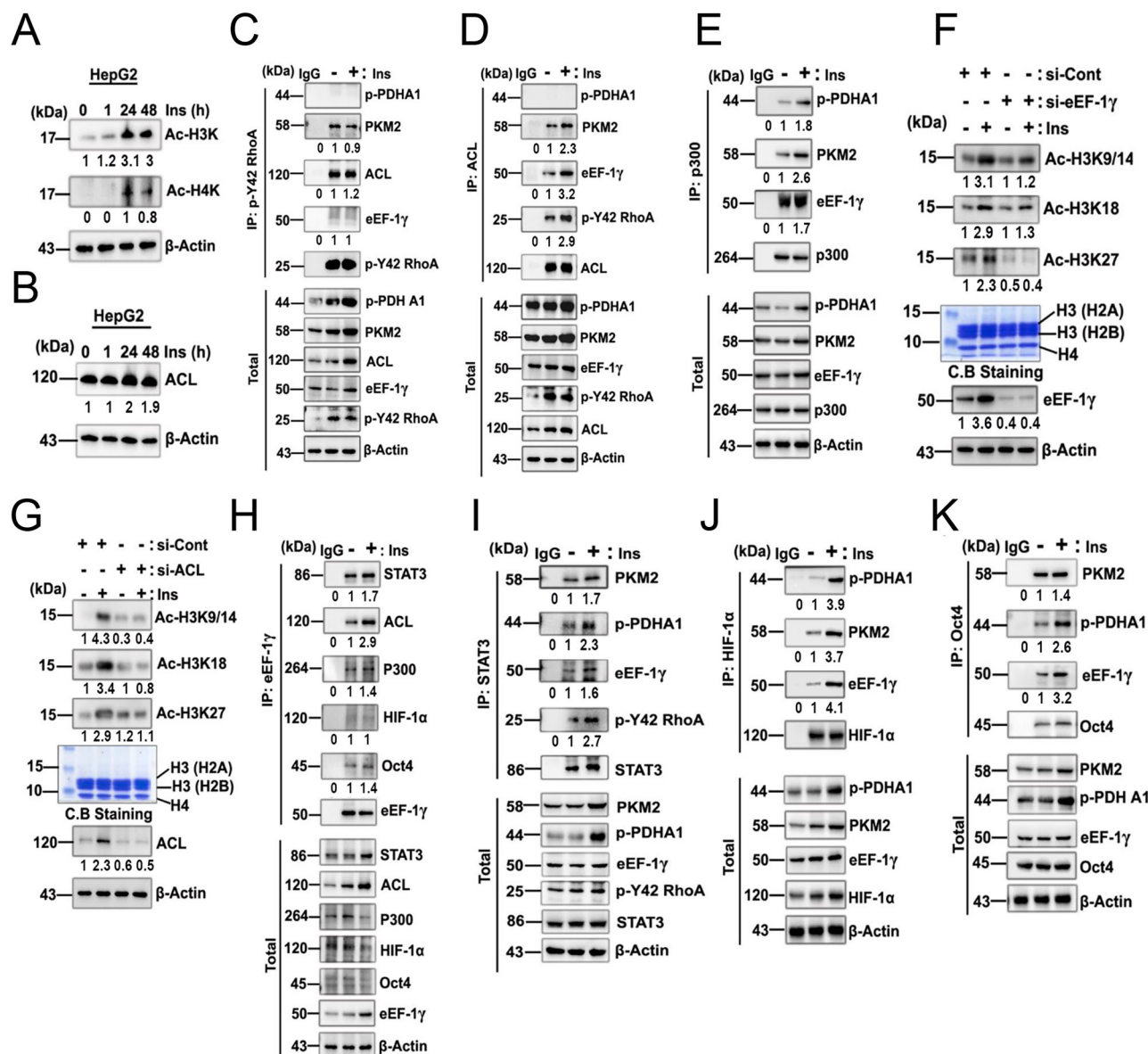
Fig. 3 | eEF-1γ is involved in histone acetylation in the nucleus. A, **B** HepG2 cells were treated with insulin (100 nM) for the indicated period, then the levels of acetylated histone H3K and H4K, and ACL were detected by western blotting. **C**–**E** HepG2 cells were stimulated by insulin (100 nM) for 48 h, then co-immunoprecipitation of p-Y42RhoA (**C**), ACL (**D**) and p300 (**E**), respectively, was performed and bound target proteins species were detected by western blotting. **F**, **G** HepG2 cells were transfected with si-eEF-1γ (**F**) and si-ACL (**G**), respectively, and then followed by insulin administration with 100 nM for 24 h. Histone proteins were isolated by acid extraction methods overnight at 4 °C, and stained with Coomassie-blue staining (middle panel). Acetylated histones, including acetylated-H3K9/14, -H3K18, and -H3K27 histone were detected by western blotting (upper panel). Transfection efficiency of si-eEF-1γ and si-ACL levels were tested by western blotting (lower panel). **H**–**K** HepG2 cells were stimulated with insulin (100 nM) for 48 h, and immunoprecipitation of eEF-1γ (**H**), STAT3 (**I**), HIF-1α (**J**), and Oct4 (**K**) was performed using each antibody, and the target bound proteins were detected by western blotting. Western blot data are representative of at least three ($n = 3$) independent experiments.

each antibody (Fig. 4I). Using protein prediction site (https://pridictprotein.org) and PyMol program (version 4.6.0), we predicted DNA binding domains in PDHA1, PKM2 and eEF-1γ. We found that PDHA1, but not PKM2 and eEF-1γ was predicted to have several domains to bind with DNA (Fig. 4J and Supplementary Fig. S2). Consequently, we speculate that PDHA1 may be a major DNA binding component among PDHA1, PKM2 and eEF-1γ, and that PDHA1 directly or indirectly interacts with other transcription factors and RNA polymerase. Next, we investigated whether insulin induces histone acetylation in RBP4 promoter region. ChIP-PCR demonstrated that insulin promotes acetylation of H3K27, H3K18, and H3K9/14, suggesting that RBP4 expression by insulin is associated with histone acetylation of RBP4 promoter (Fig. 4K). Furthermore, treatment with si-RBP

transfection increased glucose consumption in the media, suggesting that RBP4 inhibits glucose usage by HepG2 cells (Fig. 4L).

Insulin effect on eEF-1γ in normal rat liver tissue
Since the expression of p-PDHA1 in HepG2 cells has been reported to be different that in normal liver tissue in response to insulin, we investigated whether insulin regulates the differential expression levels of p-PDHA1, PKM2, PKM1, eEF-1γ, and RBP4 between HepG2 cells and normal rat liver tissue. In normal rat liver tissue, insulin treatment markedly reduced p-PDHA1 levels, and PKM1 but not PKM2 was significantly expressed. However, in HepG2 cells, insulin enhanced the levels of p-PDHA1 and PKM2, but did not affect PKM1 expression (Fig. 5A). Consistent with these findings, insulin also attenuated p-PDHA1 levels in primary hepatocytes,
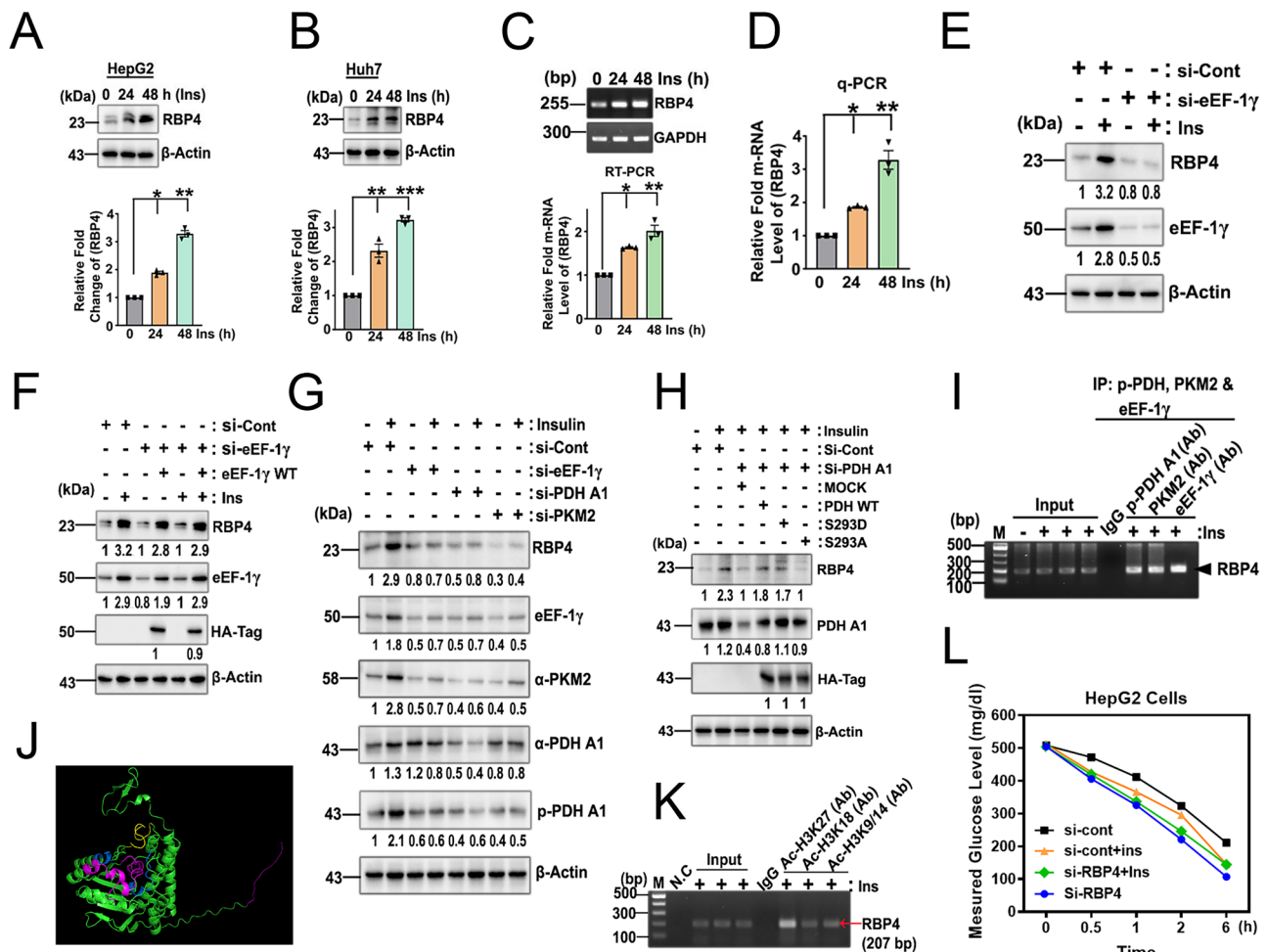
Fig. 4 | eEF-1γ regulates RBP4 expression. **A**, **B** RBP4 protein levels were analyzed by western blotting in insulin-treated HepG2 and Huh7 cells, with quantification shown in the bottom panel respectively. **C**, **D** RBP4 mRNA levels were measured by RT-PCR (**C**) and RT-qPCR (**D**) in 100 nM insulin-stimulated HepG2 cells as indicated time periods. **E**, **F** RBP4 expression was examined in HepG2 cells after si-eEF-1γ knockdown (**E**) and reconstitution with eEF-1γ WT (**F**) by western blot analysis. **G** RBP4 levels were assessed in insulin-stimulated HepG2 cells transfected with si-PDHA1, si-eEF-1γ, or si-PKM2 followed by the western blot analysis. **H** PDHA1 knockdown and reconstitution with WT, S293D, or S293A mutants in HepG2 cells were analyzed for the expression of RBP4, PDHA1 or HA-Tag by western blotting. **I** Chromatin was immunoprecipitated with eEF-1γ, p-PDHA1,

and PKM2 antibodies, and ChIP-PCR was performed using RBP4 primers targeting its promoter region. **J** PDHA1 (NCBI reference sequence: NP_00275.1) DNA-binding domains were predicted (https://predictprotein.org) and visualized using PyMol (version 4.6.0). **K** ChIP-PCR with acetylated-histone antibodies was performed on the RBP4 promoter in 100 nM insulin-treated HepG2 cells for 24 h. **L** HepG2 cells were transfected with si-RBP4 or control siRNA for 24 h, followed by insulin treatment (100 nM). Glucose levels in the media were measured using a kit at the indicated time points. The data are mean ± SD of three independent experiments (*$p < 0.05$; **$p < 0.01$, and ***$p < 0.001$) in case without particular remark. Western blot data are representative of at least three (n = 3) independent experiments.

while promoting the expression of eEF-1γ, RBP4 and PKM1, but not PKM2 (Fig. 5B). Additionally, insulin treatment increased ACL levels in normal rat liver tissues (Fig. 5C). Insulin also increased histone acetylation in normal rat liver tissue, including H3K18, H3K27 and H3K9/14 (Fig. 5D). Interestingly, we found that eEF-1γ also co-immunoprecipitates with ACL, p300, STAT3 and HIF-1α in normal rat liver tissue (Fig. 5E). In normal rat liver tissue, insulin increased the co-immunoprecipitation of p-PDHA1 with eEF-1γ (Fig. 5F). In normal rat liver tissue, PKM1 co-immunprecipitated with eEF-1γ, but not with p-PDHA1 (Fig. 5G). The most distinct feature between hepatocellular carcinoma cells and normal hepatocytes in the signaling pathway is PDHA1 phosphorylation. We presented schematic illustration of the protein complex (Fig. 5H).

eEF-1γ regulates cell proliferation, migration and Invasion
Although eEF-1γ has been previously reported as on-crucial for the translation step, knock-down of eEF-1γ with siRNA resulted in attenuated cell proliferation in HepG2, Huh7 and Hepa1c1c7 cells (Fig. 6A–C). These findings were consistent with si-eEF-1γ also

abolishing the expression of c-Myc and cyclin D1, while transfection with eEF-1γ WT restored their expressions (Fig. 6D). In addition, si-eEF-1γ reduced HepG2 cell migration in the wound healing assay (Fig. 6E). These results were further supported by si-eEF-1γ attenuating the expression of EMT markers, including ZEB1, N-cadherin, vimentin, and Snail1, while promoting E-cadherin expression (Fig. 6F). eEF-1γ may be participated in the regulation of ZEB1 expression through eEF-1γ association with the promoter of ZEB1, resulting in the expression of ZEB1 and cell migration (6 G). Furthermore, insulin attenuated E-Cadherin-Luciferase (Luc) activity. Conversely, when si-eEF-1γ upregulated E-Cadherin-Luc activity while reconstituted eEF-1γ WT again attenuated its activity, suggesting that eEF-1γ is essential for the EMT process induced by insulin (Fig. 6H).

Next, we conducted a series of experiments to investigate the role of RBP4 in cell migration, invasion and proliferation. Our findings revealed that insulin triggered an increase in RBP4 expression, leading to the secretion of a portion of the RBP4 into the surrounding media (Fig. 6K). To further understand the involvement of RBP4 in cell migration, we
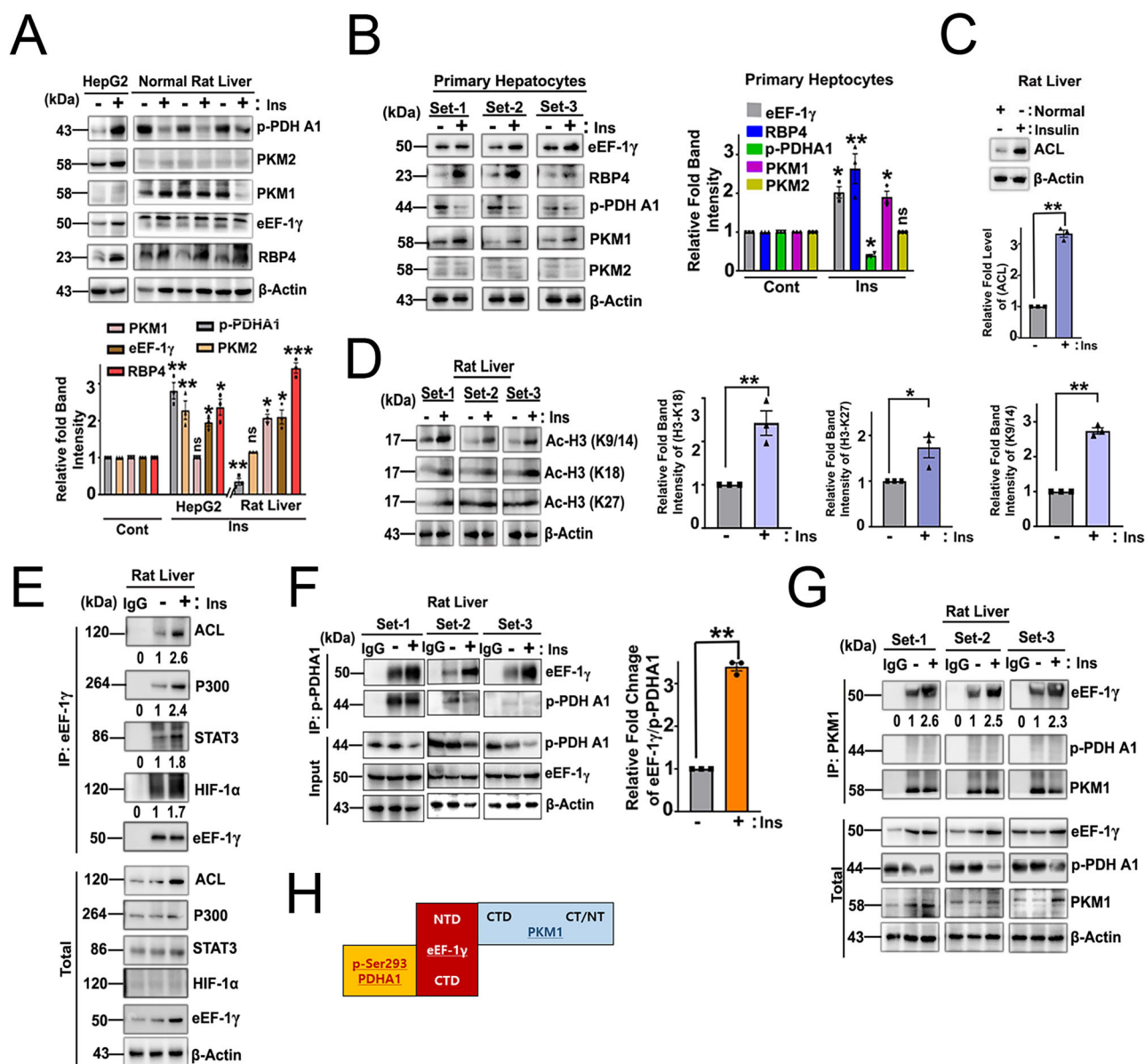
Fig. 5 | Insulin effect on eEF-1γ in normal rat liver tissue and primary hepatocytes. A HepG2 cells were stimulated with Insulin (100 nM) for 24 h, and rat liver were injected with insulin (10 U/kg body weight) for 3 h, then protein species were measured by western blotting. **B** Primary hepatocytes were isolated from mouse liver and grown in DMEM media, then treated with insulin (100 nM) for 24 h, several proteins were measured by western blotting. **C** Relative ACL levels were detected by immunoblotting in rat liver tissues treated with insulin (10 U/kg body weight) for 3 h. **D** Acetylated histone proteins, including actylated-H3K9/14, -H3K18 and

-H3K27, were measured by western blotting from rat liver tissues treated with insulin (10 U/Kg body weight) for 3 h. **E–G** p-PDHA1, PKM1, or eEF-1γ was immunoprecipitated using each antibody from rat liver tissues administered by insulin (10 U/Kg body weight) for 3 h, and target proteins were measured by western blotting. The data are mean ± SD of three independent experiments (*$p < 0.05$; **$p < 0.01$, and ***$p < 0.001$) in case without particular remark. Western blot data are representative of at least three ($n = 3$) independent experiments. **H** Schematic illustration of the complex of p-Ser293 PDH, eEF-1γPKM1 is shown.

administered exogenous RBP4 antibody and conducted si-RBP4 transfection. Notably, both approaches effectively suppressed insulin-induced cell migration, supporting the role of RBP4 in regulating cell migration, as demonstrated by the wound healing and matrigel invasion assay (Fig. 6I, J, respectively). Consistent with these findings, transfection with RBP4 WT restored the reduced migration caused by si-RBP4 knock-down (Fig. 6I, J). Regarding cell proliferation, treatment with an exogenous RBP4 antibody or si-RBP4 transfection significantly inhibited cell proliferation, whereas RBP4 WT transfection enhanced proliferation in response to insulin or FBS (Fig. 6L, M, respectively). Of note, our study also indicated that knocking down RBP4 with siRNA had a direct impact on the reduced levels of tested proteins, including p-Tyr42 RhoA, RhoA, and ROCK1/2 (Fig. 6N).

eEF-1γ is involved in tumorigenesis

We investigated the role of eEF-1γ in tumorigenesis using siRNA knock-down in 4T1 cells, and the results were compelling. Knock-down of eEF-1γ with siRNA prevented tumorigenesis of 4T1 cells, as evident from the outcomes (Fig. 7A–D). On the other hand, when we reconstituted eEF-1γ WT, tumor progression was restored, indicating the crucial role of eEF-1γ in tumorigenic process. Furthermore, our analysis of liver tumor tissues showed elevated levels of eEF-1γ, p-PDHA1, and PKM2 compared to adjacent areas surrounding the tumor mass (Fig. 7E–H and Supplementary Table 1). This observation suggests a potential association of these molecules with liver tumorigenesis. To explore the clinical relevance of eEF-1γ expression in liver cancer patients, we performed Kaplan-Meier survival analysis based on the eEF-1γ levels in liver tissue. The analysis revealed that patients with high
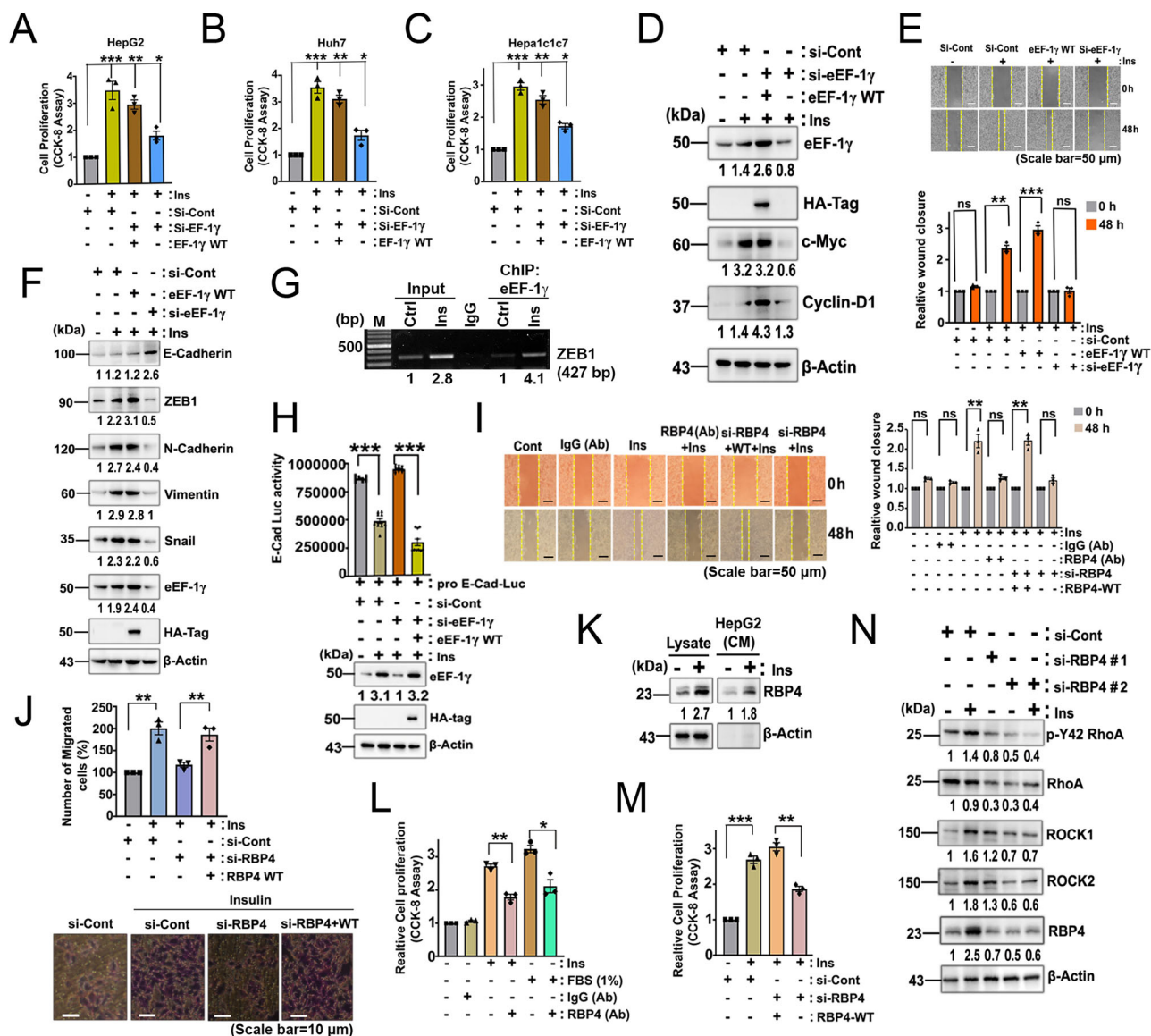
Fig. 6 | eEF1-γ regulates cell proliferation, migration and invasion upon insulin stimulation. A–C HepG2, Huh7 and Hepa1c1c7 cells were transfected with si-eEF-1γ then reconstituted with eEF-1γ WT, finally cell proliferation was measured by using CCK-8 assay, stimulated by insulin (100 nM) for 24 h. **D** HepG2 cells were transfected with si-eEF-1γ, then reconstituted with eEF-1γ WT, and activated with insulin (100 nM) for 48 h. c-Myc and cyclin D1 were determined by western blotting.(**E** Knockdown of eEF-1γ with siRNA in HepG2 cells was first performed, then reconstituted with eEF-1γ WT, and finally wound healing was measured after 48 h in response to insulin (100 nM) administration. **F** Knockdown of eEF-1γ with siRNA in HepG2 cells was first performed, then reconstituted with eEF-1γ WT, and EMT marker proteins were measured by western blotting upon insulin (100 nM) stimulation for 24 h. **G** ChIP-PCR experiments were conducted on HepG2 cells exposed to insulin (100 nM) for 24 h, Chromatin was immunoprecipitated with eEF-1γ and primers specific for covering ZEB1 promoter region. **H** HepG2 cells were transfected with E-cadherin Luc plasmid, then transfected with si-eEF-1γ, and then eEF-1γ WT was reconstituted. The E-cadherin Luc activity was measured by Promega galactosidase assay (Madison, WI

53711-5399, USA) in response to insulin (100 nM) for 24 h. **I** HepG2 cells were transfected with si-RBP4, then reconstituted with RBP4 WT, or administered with control and RBP4 antibodies. Cell migration using wound healing assay was determined in response to 100 nM insulin for 48 h. **J** HepG2 cells (2 × 10⁴ cells) were seeded in 24-well coated invasion chamber containing Matrigel matrix then transfected with si-RBP4 and reconstituted with RBP4 WT. Finally, invaded cells were measured by staining with crystal violet. **K** Lysates and conditioned media (CM) of HepG2 cells stimulated with insulin (100 nM) for 24 h were analyzed by western blotting with RBP4 antibody. **L, M** HepG2 cells were treated with 1 μg RBP4 antibody or control IgG antibody (**K**). HepG2 cells were transfected with si-RBP4, then reconstituted with RBP4 WT (**M**), and cell proliferation was assessed with CCK-8 assay in response to insulin (100 nM) stimulation for 48 h. **N** HepG2 cells transfected with two types si-RBP4 followed by insulin (100 nm for 24 h) and target protein species were detected by western blotting. The data are mean ± SD of three independent experiments (*$p < 0.05$; **$p < 0.01$, and ***$p < 0.001$) in case without particular remark. Western blot data are representative of at least three ($n = 3$) independent experiments.

eEF-1γ expression had significantly poorer survival probability compare to those with lower eEF-1γ levels (Fig. 7I–K). This indicates that eEF-1γ expression might serve as a prognostic marker in liver cancer.

Discussion

The insulin signalling pathway is a well-studied mechanism that plays a critical role in regulating glucose homeostasis and cell proliferation. Upon

binding to its receptor, insulin activates downstream signalling cascades, including insulin receptor substrate (IRS), phosphatidylinositol-3-kinase (PI3K), Akt/protein kinase B (PKB), glycogen synthase kinase-3β (GSK-3β) and mTOR, ultimately leading to uptake glucose uptake and reduction of blood glucose level. In addition, insulin has been shown to promote cell proliferation through the Ras/MAPK/ERK pathway[28–30]. Notably, in our previous study, we found that insulin reduced p-PDHA1 levels in normal
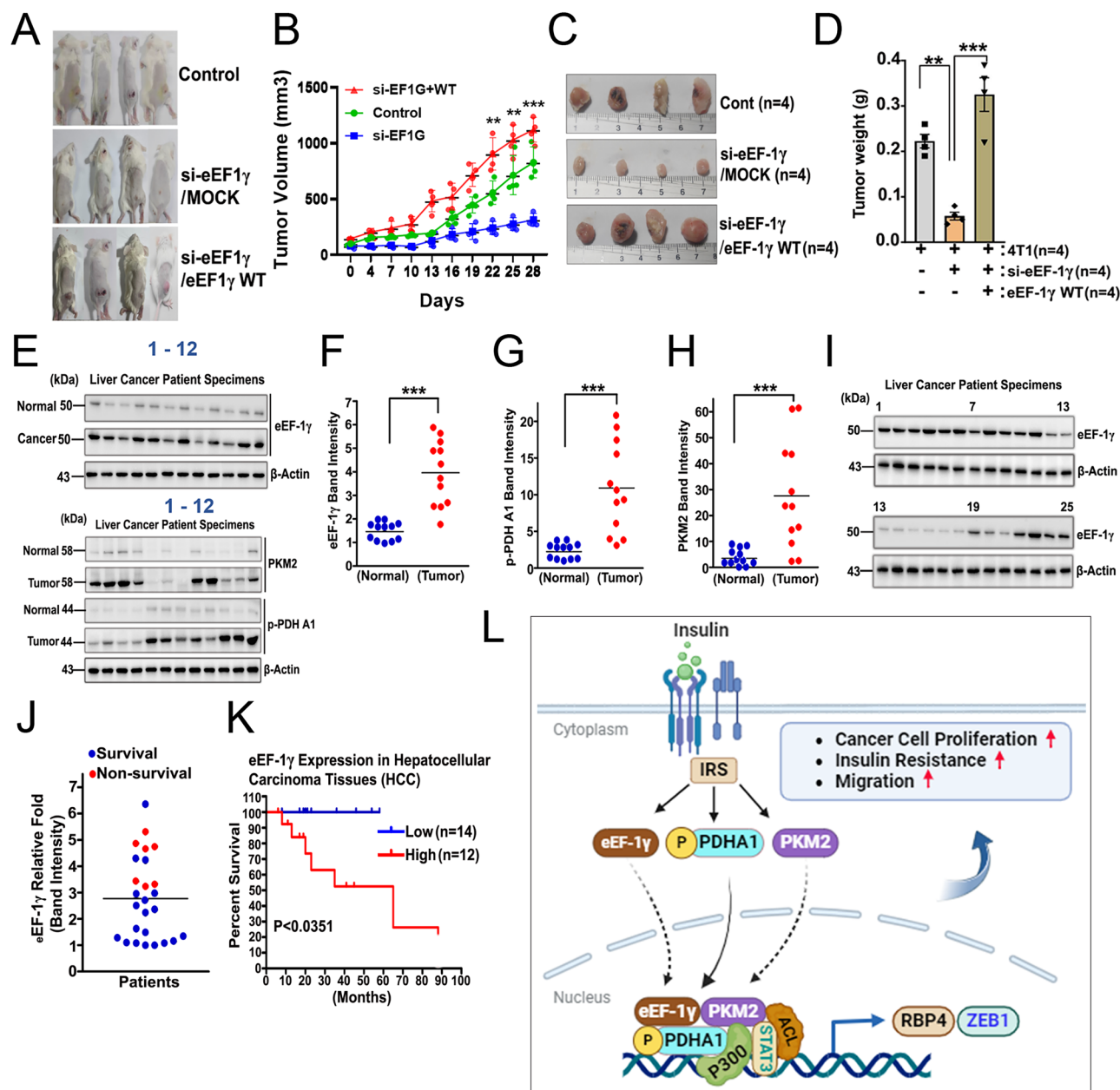
Fig. 7 | eEF-1γ is implicated in tumorigenesis, and its high expression is associated with poorer survival. A Representative images of BALB/c mice (*n* = 4) harboring tumors of 4T1 cells which were transfected with si-eEF-1γ and reconstituted with eEF-1γ WT were presented. PMA (20 μM, 20 μl) was applied to the surface of regions injected with the 4T1 cells every day. **B** The volume of tumor masses was measured every three days. **C, D** The representative tumor mass and weight of cancer cells harboring si-eEF-1γ or si-eEF-1γ/eEF-1γ WT were presented. **E** eEF-1γ, p-PDHA1 and PKM2 levels in human liver samples liver cancer patients were measured by western blotting. **F–H** Relative protein band intensities of eEF-1γ, p-PDHA1 and PKM2 levels in liver cancer patient samples were shown in survival (blue) and non-survival patients (red),

respectively. Normal tissues were obtained from surrounding region of tumor. **I** eEF-1γ levels in human liver cancer patient samples in other cohort were measured by western blotting. **J** Relative band intensities of eEF-1γ levels in liver cancer patient samples were shown in survival (blue) and non-survival (red), respectively. **K** Survival probability according to the tumor-associated low and high levels of eEF-1γ in liver cancer patients were presented in Kaplan-Meier graph. **L** Proposed schematic diagram for role of eEF-1γ/p-PDHA1/PKM2 trimeric complex in cancer cells. Illustration generated by biorender.com website. The data are mean ± SD of three independent experiments (*$p < 0.05$; **$p < 0.01$, and ***$p < 0.001$) in case without particular remark. Western blot data are representative of at least three (*n* = 3) independent experiments.

liver tissue but significantly up-regulated its levels in HCC lines, including HepG2 and Huh7 cells, along with promoting cell proliferation[17]. In this study, we have identified eEF1γ to bind with p-PDHA1, leading to the formation of a trimeric complex with p-PDHA1/PKM2, which contributes to a new function of eEF1γ in regulating gene expression.

Apart from the conventional role in protein synthesis, the eEF1γ subunit has been reported to have a noncanonical functions, including the retrograde Golgi to ER transport, oxidative stress, cytoskeleton

organization, and DNA damage response[31,32]. Particularly, eEF1γ subunit have a broader impact on gene expression by interacting with various factors. For instance, it was revealed that the RNA-dependent RNA polymerase of a virus was revealed to interact with eEF-1α, β, and γ subunits[15]. Additionally, eEF1γ was found to bind with Che-1 and p53 transcripts and their promoters[33]. Another study discovered that eEF1γ, along with HAX-1 (HS1-associated protein X-1) and hRIP (human rev interacting protein), binds with 3' UTR mRNA of the vimentin gene[34]. Moreover, eEF1γ subunit

was reported to interact with RNA polymerase II and binds to the promoter region of vimentin gene[16]. The co-localization of eEF1γ and vimentin mRNAs with mitochondria suggests that vimentin may play a role in regulating mitochondria function. eEF1γ also binds to MAVS (mitochondrial antiviral-signaling protein) and is predominantly localized in the cytoplasm, partially colocalizing with MAVS in the mitochondria. Additionally, eEF1γ activates NF-κB, leading to enhanced transcription of IL-8 and IL-6[35]. In our study, we made a significant discovery by identifying that eEF1γ binds to p-PDHA1/PKM2, forming a trimeric complex that stabilizes PKM2 and p-PDHA1. Moreover, we found that eEF1γ, together with PKM2 and p-PDHA1, regulates RBP4 expression through their binding to RBP4 promoter (Fig. 4I). Furthermore, our research indicates that eEF1γ, together with p-PDHA1/PKM2, is crucial for the regulation of histone acetylation, which may be associated with gene expression regulation (Fig. 3). These findings shed light on the diverse roles of eEF1γ in gene expression regulation beyond its classical function in protein synthesis.

Studies have provided evidence that RBP4 plays a role in insulin resistance in obesity and type 2 diabetes[22,36] and is primarily secreted in the liver under normal conditions[37]. Additionally, RBP4 is co-secreted along with glucagon from pancreatic α-cells in response to a secretory stimulus. Its interaction with potent metabolic regulators, such as glucagon and glucose-dependent insulinotropic polypeptide (GIP) that regulate metabolism helps explain some of the metabolic disorders observed with RBP4 overexpression[38]. Moreover, RBP4 is associated with pancreatic adenocarcinoma (PDAC), hepatocellular carcinoma, acute myeloid leukemia, and breast cancer[39–42]. Furthermore, RBP4 has been implicated in cancer development, promoting tumorigenesis and colon cancer self-renewal through its receptor STRA6[27]. In ovarian cancer cells, RBP4 overexpression has been found to up-regulate migration and proliferation through the activation of RhoA/ROCK, MMP2 and MMP9 expression, as well as Cyclin D1 expression[43]. Moreover, exogenous RBP4 has been associated with promoting metastasis, invasive and cologenic potential, endothelial dysfunction, and impairment of blood vessel[44]. Conversely, there has been a report indicating that RBP4 is reduced in HCC, and low RBP4 expression is relevant to advanced tumor stages and grades[45]. Although it remains controversial whether high RBP4 levels are associated with cancers, RBP4 may be still associated with specific types of cancers. Based on RBP4 protein expression levels, most liver and renal cancers display moderate to strong cytoplasmic immunoreactivity, whereas other malignant tissues are generally weakly or negatively stained (reference: Expression of RBP4 in cancer, The Human Protein Atlas).

Therefore, we propose the following signaling pathway and mechanism of insulin in HCC. Insulin triggers Ser293 phosphorylation of PDHA1, leading to the formation of the e-EF-1γ/p-PDHA1/PKM2 trimeric complex. Subsequently, this complex translocates into the nucleus, where it regulates histone acetylation by recruiting p300 acetyltransferase and ACL to specific gene promoters, notably RBP4. As a consequence, elevated insulin levels contribute insulin resistance through the upregulation of RBP4, a process regulated by eEF-1γ. Furthermore, RBP4 has been linked to HCC progression, adding significance to these findings. Hence, we propose eEF-1γ plays a crucial role in stabilizing both p-PDHA1 and PKM2, with p-PDHA1 being pivotal for PKM2 stability. Moreover, our research indicates that eEF-1γ is essential for cell proliferation and migration. In conclusion, insulin fosters cancer cell proliferation, migration, and tumorigenesis in hepatocellular carcinoma cells.

Methods
Materials
Human recombinant insulin (Cat: INSL16-N-5) were obtained from Alpha Diagnostic International (ADI) (San Antonio, TX, USA). Isopropyl β-D-thiogalactoside (IPTG) were purchased from Sigma-Aldrich Co. (St. Louis, MO, USA). Y27632 was obtained from Calbiochem (La Jolla, CA, USA). Tat-C3 cDNA plasmid (Tat-C3 fusion protein containing Tat-peptide and C3 toxin) were purified by using BL-21 competent cells as previously

reported[46]. Tat-pDHA1 peptide was synthesized from Peptron (South korea). LB broth with high salt (MB-L4488) and skim milk powder (MB-S1667) were from MBcell (Seoul, Korea). Alexa flour 488 goat anti-mouse IgG, 4'6-diamidino-2-phenylindole (DAPI) and ProLong Gold Antifade mounting solution, Alexa flour-568 and Alexa flour-594 reagents were obtained from Molecular Probes (Eugene, OR, USA). Transfection reagent JetPRIME DNA/siRNA were purchased from Polyplus-transfection (Seoul, Korea). Glutathione (GSH)-sepharose 4B/agarose and Protein A/G-agarose beads were from Amersham Biosciences (Piscataway, NJ, USA). Secondary HRP-conjugated antibody goat anti-rabbit and goat anti-mouse IgG were purchased from Enzo Life Sciences (Farmingdale, NY, USA). Finally, most commonly antibodies were used for this study were shown in supplementary table 1.

Cell culture
Human hepatocellular carcinoma cell lines HepG2 and Huh7 were obtained from the Korean Cell Line Bank (Seoul, Korea). The Hepa1c1c7 mouse hepatoma cell line and the 4T1 mouse breast cancer cell line was purchased from the American Type Culture Collection (ATCC, USA). All cells were cultured at 37 °C in a humidified atmosphere containing 5% CO_2 using Dulbecco's Modified Eagle Medium (DMEM) (Welgene, Inc., Korea) supplemented with 5% heat-inactivated fetal bovine serum (FBS), 100 U/mL penicillin, and 100 μg/mL streptomycin. Each cell line was tested for mycoplasma contamination (see Supplementary Fig. S3), and a complete list of additional cell lines used in this study is provided in Supplementary Table 2.

Protein extraction and western blot analysis
Cells were seeded in 6-well plate 1 x 10⁶ cells per well. The treated cells washed once with 1 X PBS and lysed on ice in radioimmunoprecipitation assay (RIPA) buffer (20 mM Tris-HCl pH 7.5, 1 mM EDTA, 1% (v/v) NP-40, 150 mM NaCl and 1 mM $MgCl_2$) including fresh cocktail of protease and phosphatase inhibitors (Abbkine, Wuhan, China). The total protein concentration of the cell extracts was determined using the Pierce BCA Protein Assay Kit (Thermo Fisher Scientific, Rockford, IL, USA). Aliquots of the extracts (20 μg of protein) were then separated via 10-14% SDS-PAGE gels. Target proteins band were visualized by enhanced chemiluminescence (ECL) (Luminata Forte) (Millipore) and then detected with Chemisuper & Chemiluminesent imaging system FUSION FX-Western Blot. (Vilber Lourmat)[47]. Antibodies used for Western blotting and IP were listed in supplementary table 3.

Protein identification by peptide mass fingerprinting (PMF)
HepG2 cells were grown in DMEM media containing 5% FBS with 1% penicillin-streptomycin. The cells were incubated without serum for 12 h, then treated with insulin (100 nM) and then harvested. Bead-conjugated recombinant GST-PDHA1 S293D phospho-mimetic protein was purified and incubated with a nuclear fraction extract of HepG2 cells at 4 °C. The beads were washed several times and bound proteins were extracted with SDS-PAGE sample buffer. The samples were loaded into SDS-PAGE and stained with Coomassie-blue. We selected a specific protein band, which associated with GST-PDHA1 S293D, and identified the proteins using MALDI-TOF analysis (Microflex LRF 20, Bruker Daltonics, Germany) (Genomine Inc., Pohang, South Korea) according to Fernandez et al.[48].

Immunoprecipitation
Cells at 1 x 10⁷ were washed with 1XPBS and lysed on ice for 30 min in modified RIPA buffer (150 mM NaCl, 50 mM Tris-HCL, pH 7.4, 1% NP-40) containing a fresh cocktail of protease and phosphatase inhibitors (100X, Abokine). Cell lysates were pre-cleared with control IgG for 1 h and then incubated with a specific primary antibody (2 μg) overnight at 4 °C. Protein A/G beads (25 μl slurry) were used to capture of target proteins. Finally, samples were eluted by the addition of 40 μl 5X SDS sample buffer, and separated on SDS-PAGE gels for immunoblot analysis[47].

Cell proliferation inhibition checked by CCK-8 assay

Cells at 1×10^5 were cultured in 12-well plates containing DMEM media, then incubated without serum for 12 h, then stimulated either with insulin 100 nM or 1% FBS to cells and then incubated for 24–48 h at 37 °C in CO_2 incubator. For colorization of living cells, 5–10 µl of CCK-8 reagent (WST-8: [2-(2 methyoxy-4-nitrophenyl0-3-(4-nitrophenyl)-5-(2,4-disulfophenyl)-2H-tetrazolium, monosodium] from Quanti-Max-WST-8 Cell Viability assay kit (Biomax, Cat: QM 2500) and finally, fluoresence was measured at 450 nm in a spectrophotometer and viability were plotted using GraphPad Prism 4 software (GraphPad). To ensure reproducibility, these assays were repeated three times.

Recombinant GST-fusion proteins purification

EEF-1γ cDNA clone (Human) was a gift from Dr. Sung-Hoon Park, professor (Korea Institute of Toxicology, Daejeon, Korea) and PKM2 cDNA clone (Human, hMU009169) was purchased from Korea Human Gene Bank (Seoul, Korea). Domains of PKM2, including N-terminal, A1-, B-, A2- and C- terminal domains containing EcoR1 and XhoI restriction sites were inserted to pGEX4T1 plasmid by using EcoR1 and XhoI restriction sites. To construct the domains, primers containing individual primers (5' and 3' ends of each individual primer) were manufactured from Bioneer (Daejeon, Korea) and constructs were synthesized through PCR. Recombinant GST-PKM2 of full length and domains, as well as GST-eEF-1γ WT, and GST-eEF-1γ domains in pGEX4T1 plasmid were expressed in *E. coli BL-21*. Isopropylthio-galactosidase (IPTG) 0.5 mM was added to *E. coli BL21* to induce protein expression. The target recombinant proteins were purified using glutathione (GSH)-Sepharose 4B beads.

Transfection of plasmid DNA, siRNA, overexpression, knockdown and control vectors

Plasmid DNA and small interfering RNA (siRNAs) against RBP4 (sc-44071), PDHA1 (sc-91064), PKM2 (sc-62820) as well as control siRNA-A (sc-37007, sc-44232) were purchased from Santa Cruz Biotechnology. In addition, siRNAs for eEF-1γ, PDHA1 and RBP4 were purchased from Bioneer Inc. (Daejeon, South Korea). The cells were seeded and incubated to 40%–50% confluency and transfected with siRNAs using either Lipofectamine 3000 (Invitrogen) or JetPrime polyplus-transfection reagent according to the manufacturer's instructions (Seoul, Korea). Briefly, 50 to 80 nM of each individual siRNAs were mixed with transfection reagent and were followed incubated for 15–20 min at RT, and then added to the cells in dropwise. For reconstitution or co-transfection with plasmid DNA (2 µg/well), cells with 60% to 70% confluency were used. The cells were then incubated for the optimum time period and then changes of protein expression or proliferation was measured by western blot analysis or CCK-8 assay, respectively.

Site-directed mutagenesis

Human pCMV6-XL5 PDHA1 cDNA construct was purchased from OriGene Technologies (Rockville, MD, USA). Mutant PDHA1 S293D constructs were prepared from pCMV6-XL5 PDHA1 WT by using site-directed mutagenesis kit (Intron Biotechnology, Seongnam, Korea). Each individual primer was designed with a specific point mutation as described by the manufacturer's protocol and synthesized from Bioneer Inc. (Daejeon, South korea). Mutant PKM2 K305R, and PKM2 K305Q constructs were constructed by using the same protocol[4].

Cytosolic and nuclear fractions isolation

Insulin was treated at 100 nM for 48 h to HepG2 cells, the cells were washed once with 1 X PBS and harvested, and then were lysed in cytoplasmic extraction reagent I (CER-I, 200 µl, NE-PERTM Nuclear and Cytoplasmic Extraction Reagents, Thermo Scientific, Rockford, IL USA) plus protease inhibitors at $14,000 \times g$ for 15 min at 4 °C. The total cytoplasmic proteins were collected to a new tube and concentration of the proteins were determined using the Pierce BCA Protein Assay Kit (Thermo Fisher Scientific, Rockford, IL, USA). Remaining cell pellets were washed once with

buffer before adding nuclear extraction reagent (CER-II, 11 µl) plus protease inhibitor to the cell pellet and then vortex vigorously 15 s in every 10 min of total 40 min in ice. Nuclear proteins were collected by centrifugation at $16,000 \times g$ for 15 min at 4 °C and kept in aliquots of each fraction. Around 20 µg of each cytosolic and nuclear proteins were measured with Western blotting[49].

Immunostaining of cells

Cells were cultured and stimulated by insulin for 24 h then fixed in 4% paraformaldehyde for 10 min, neutralized with 20 mM glycine for 10 min, and then washed three times with 1 X PBS containing 0.1% Triton X-100 (PBST). The samples were incubated with the specific primary antibody (1:100) overnight at 4 °C. The cells were washed and primary antibody against eEF-1γ was administered and then recognized by an Alexa Fluor 488-conjugated secondary antibody at 1:100 ratios (green-color emission) for 2 h at room temperature (RT). DAPI (1:300) was also administered for 10 min to visualize the nuclei, then the cells were washed and mounted on the slide. Confocal images were taken by using a confocal microscope (ZEISS ZEN, Oberkochen, Germany)[50]. Confocal image processing was performed using ZEISS ZEN 3.7 software.

Monolayer wound healing assay

HepG2 cells were seeded to 50%–60% confluency then transfected with siRNAs or co-transfected with plasmid DNAs, then incubated for 24 h with or without insulin stimulation. Around 90% confluent cells were used for wound healing assay. Briefly, a 1 ml sterile pipette tip was used to scratch the cell monolayer to make wound across the center of the well. The cells were incubated for 48 h, monolayer wound widths were captured randomly and analyzed in images with a light microscope (Axiovert 200, Zeiss and Adobe Photoshop 7). The relative fold of monolayer wound closure was calculated following the previous methods (Biomedicine, 2022).

Trans-well Invasion Assay

The Matrigel invasion assay was performed using 8-µm pore polycarbonate membrane inserts (Corning, USA) in 24-well plates, coated with 0.5 mg/ml Matrigel (BD Biosciences, MA). HepG2 cells were subjected to RBP4 knockdown using si-RNA, followed by reconstitution with WT-RBP4 transfection and then 1×10^5 cells in 200 µl serum-free medium were seeded in the upper chamber. After complete attachment the cells undergoes with 100 µM insulin treatment, while the lower chamber contained serum depleted medium. After 48-hour insulin treatment at 37 °C, membranes were fixed in 75% methanol for 30 min. Non-invading cells were removed, and invading cells were stained with 0.5% crystal violet (20% methanol) for 60 min. Cells were counted in 10 fields per membrane under an inverted microscope. Experiments were performed in triplicate.

Chromatin immunoprecipitation PCR (ChIP-PCR)

We followed Abcam's protocol for ChIP assay. Insulin was treated at 100 nM for 48 h to HepG2 cells, and then cells were crosslinked by 1% formaldehyde at RT for 30 min and the crosslinking reaction was stopped by adding 125 mM glycine/PBS, followed by successive three washes. Cells were collected by centrifugation at $1000 \times g$ and ChIP lysis buffer (50 mM HEPES-KOH pH 7.5, 140 mM NaCl, 1 mM EDTA pH 8.0, 1% Triton X-100, 0.1% Sodium Deoxycholate and 0.1% SDS) containing fresh protease inhibitors was added to cell pellet (750 µl/1 X 10^7 cells) for lysis. Cross linked chromatin of samples was shredded to 200 to 1000 bp fragments by sonication. Cell debris were removed by centrifugation with $8000 \times g$ at 4 °C for 5 min, and the supernatant containing chromatin was transferred to a new tube. Samples then pre-cleared with control IgG and immunoprecipitation was performed with anti-eEF-1γ antibody overnight. Bead-conjugated protein-A/G precipitated antibody-conjugated eEF-1γ and beads were washed properly and eluted the samples with dilution buffer. DNA cross-links were reversed and bound proteins were digested by using proteinase K-glycogen and heating at 65 °C overnight. Bound DNA was purified from the samples by using phenol:chloroform extraction and fragmented DNA

were sequenced in Ebiogen Inc. (Seoul, Korea). Primers of RBP4 including the target promoter region for ChIP-PCR to validate the ChIP-Seq data by using the information in UCSC Genome Browser (Human GRCh38/hg19) as well as for the promoter of ZEB1 is located on human chromosome 10 spanning positions 31,318,016–31,319,215, and the primer sequences of both genes (supplementary table 3-1) were synthesized from Bioneer (Daejeon, Korea).

RNA isolation, RT-PCR and RT-qPCR

Total RNA was isolated from HepG2 cells by using TRIzol reagent (Applied Biosystems/Ambion). The concentration of the extracted RNA was measured by Nano Drop (Thermo Scientific, Waltham, Massachusetts, United States). The cDNA was prepared from isolated RNA using M-MLV reverse transcriptase enzyme through reverse transcription (NEB-UK, Hitchin, UK). The details procedure of isolation of RNA as well as making cDNA from RNA are followed the previous methods[17]. The cDNA was then used for RT-qPCR (real-time qPCR) quantification using an Applied Biosystems Step one plus PCR system. PCR primers of GAPDH were used for analysis as house-keeping control gene. For measuring RBP4, mRNA levels, primer sequences were designed (supplementary table 3-2) and measured by RT-PCR. Agarose gels (1%) containing ethidium bromide were used to run the PCR products and the stained DNA were visualized by Gel Doc imaging system (FUSION FX-Western Blot, Vilber Lourmat).

Analysis of band intensity and survival probability of human liver cancer patients

A statement confirming that informed consent was obtained. All ethical regulations relevant to human research participants were followed. The liver (human) normal and cancer tissue specimens were collected from Pusan National University Hospital (Pusan, Korea). The collection of cancer tissue samples (supplementary table 4) was approved and evaluated by the authority of National Cancer Center of Korea (NCCK). Around 25 µg of proteins were isolated from liver normal and cancer tissues, and then separated on SDS-PAGE for western blot analysis: we measured eEF-1γ, p-PDHA1 and PKM2 protein expression from normal and cancer tissue samples with western blotting, calculated the relative band intensity, and then plotted them into a graph. From the results, we created Kaplan-Meier survival graph, based on patient's information which were found from KOSTAT system of Korean Government database (Korean Statistical Information Service, KOISIS). This experiment was approved by authority of the Institutional Review Board (IRB) at Hallym University (Chuncheon, Korea). According to KOSTAT database, the survival and non-survival patients were denoted as 1 or 0, respectively, finally survival probability graphs were generated by the GraphPad Prism 8 program.

Preparation of rat liver samples

All animal experiments were approved by the Animal Care and Use Committee of Hallym University (approval number: Hallym2017-3 and 2022-6), Chuncheon, South Korea. We have complied with all relevant ethical regulations for animal use. Sprague Dawley Rats (Female, around 300 g of weight) were obtained from Samtako (Osan, Korea) and 1 ml insulin (10 U/kg body weight) with 0.9% saline injected in an intra-peritoneal cavity of rats. Briefly, only 1 ml 0.9% saline were injected for control groups of three rats. Rats were sacrificed using isoflurane anesthesia, after 2 h insulin stimulation and rat livers were isolated with I X PBS perfusion to remove all bloods. Approximately, 25 µg of protein samples were extracted from liver tissues for western blot analyses. Finally, extracted proteins were separated on SDS-PAGE and analyzed through western blot with the using of target antibody.

Xenograft experiment

All animal experiments were approved by the Animal Care and Use Committee of Hallym University (approval number: Hallym 2017-3 and 2022-6), Chuncheon, South Korea. We have complied with all relevant

ethical regulations for animal use. Female BALB/c (4–6 weeks old) mice were purchased from Samtako (Osan, Korea), for mouse allograft tumor model. In this allograft mouse model, the animal experiments were approved by the authority of Hallym University-IACUC (Institutional Animal Care and Use Committee) committee under the act number of Hallym 2021-6. The detailed procedure of allograft experiment was followed as described by Jubayer et al.[17].

Statistics and reproducibility

All the western blot experiments were conducted at least in triplicate, and some intra-assay experiments were analyzed at least in duplicate or triplicate manner. Graphical presentation and statistical analysis of data were performed using Prism 8 program (GraphPad Software, San Diego, USA). Protein bands intensities of western blotting were generated with the help of Photoshop7 cc2018 software (Adobe Inc.). Normally, statistical analysis was shown as the means ± standard deviation (SD) of at the minimum three independent experiments depending on student t-test, one or two-way ANOVA analysis ($*p < 0.05$; $**p < 0.01$, and $***p < 0.001$). The protein bands of the western blotting were presented as a representative of several experiments ($n \geq 3$), as well as bands intensity were denoted as a number in some cases.

Reporting summary

Further information on research design is available in the Nature Portfolio Reporting Summary linked to this article.

Data availability

The authors confirm that the data supporting the findings of this study are available within the article. All uncropped and unedited blot images are included as Supplementary Figs. S4–10. The source data behind the graphs in the paper can be found in Supplementary Data 1.

References

1. Clayton, P. E., Banerjee, I., Murray, P. G. & Renehan, A. G. Growth hormone, the insulin-like growth factor axis, insulin and cancer risk. *Nat. Rev. Endocrinol.* **7**, 11–24 (2011).
2. Stacpoole, P. W. & McCall, C. E. The pyruvate dehydrogenase complex: Life's essential, vulnerable and druggable energy homeostat. *Mitochondrion* **70**, 59–102 (2023).
3. Holness, M. J. & Sugden, M. C. Regulation of pyruvate dehydrogenase complex activity by reversible phosphorylation. *Biochem Soc. Trans.* **31**, 1143–1151 (2003).
4. Islam, R. et al. Insulin induces phosphorylation of pyruvate dehydrogenase through RhoA activation pathway in HepG2 cells. *FASEB J.* **33**, 2072–2083 (2019).
5. Li, Z., Yang, P. & Li, Z. The multifaceted regulation and functions of PKM2 in tumor progression. *Biochim Biophys. Acta* **1846**, 285–296 (2014).
6. Chen, X., Chen, S. & Yu, D. Protein kinase function of pyruvate kinase M2 and cancer. *Cancer Cell Int* **20**, 523 (2020).
7. Lee, Y. B. et al. Multiple functions of pyruvate kinase M2 in various cell types. *J. Cell Physiol.* **237**, 128–148 (2021).
8. Yang, W. et al. ERK1/2-dependent phosphorylation and nuclear translocation of PKM2 promotes the Warburg effect. *Nat. Cell Biol.* **14**, 1295–1304 (2012).
9. Yang, W. et al. Nuclear PKM2 regulates β-catenin transactivation upon EGFR activation. *Nature* **480**, 118–122 (2011).
10. Yang, W. et al. PKM2 phosphorylates histone H3 and promotes gene transcription and tumorigenesis. *Cell* **150**, 685–696 (2012).
11. Gao, X., Wang, H., Yang, J. J., Liu, X. & Liu, Z. R. Pyruvate kinase M2 regulates gene transcription by acting as a protein kinase. *Mol. Cell* **45**, 598–609 (2012).

Article

12. Sasikumar, A. N., Perez, W. B. & Kinzy, T. G. The many roles of the eukaryotic elongation factor 1 complex. *Wiley Interdiscip. Rev. RNA* **3**, 543–555 (2012).

13. Chang, Y. W. & Traugh, J. A. Insulin stimulation of phosphorylation of elongation factor 1 (eEF-1) enhances elongation activity. *Eur. J. Biochem* **251**, 201–207 (1998).

14. Koonin, E. V. et al. Eukaryotic translation elongation factor 1 gamma contains a glutathione transferase domain–study of a diverse, ancient protein superfamily using motif search and structural modeling. *Protein Sci.* **3**, 2045–2054 (1994).

15. Das, T., Mathur, M., Gupta, A. K., Janssen, G. M. & Banerjee, A. K. RNA polymerase of vesicular stomatitis virus specifically associates with translation elongation factor-1 alphabetagamma for its activity. *Proc. Natl Acad. Sci. USA* **95**, 1449–1454 (1998).

16. Corbi, N. et al. The eEF1gamma subunit contacts RNA polymerase II and binds vimentin promoter region. *PLoS One* **5**, e14481 (2010).

17. Hossain, A. J. et al. Pyruvate Dehydrogenase A1 Phosphorylated by Insulin Associates with Pyruvate Kinase M2 and Induces LINC00273 through Histone Acetylation. *Biomedicines* **10**, 1256 (2022).

18. Lv, L. et al. Acetylation targets the M2 isoform of pyruvate kinase for degradation through chaperone-mediated autophagy and promotes tumor growth. *Mol. Cell* **42**, 719–730 (2011).

19. Lee, Y. B. et al. Function of a complex of p-Y42 RhoA GTPase and pyruvate kinase M2 in EGF signaling pathway in glioma cells. *J. Neurochem* **169**, e16210 (2024).

20. Cap, K. C. et al. Distinct dual roles of p-Tyr42 RhoA GTPase in tau phosphorylation and ATP citrate lyase activation upon different Aβ concentrations. *Redox Biol.* **32**, 101446 (2020).

21. Arcidiacono, B. et al. Insulin resistance and cancer risk: an overview of the pathogenetic mechanisms. *Exp. Diabetes Res* **2012**, 789174 (2012).

22. Graham, T. E. et al. Retinol-binding protein 4 and insulin resistance in lean, obese, and diabetic subjects. *N. Engl. J. Med* **354**, 2552–2563 (2006).

23. Friebe, D. et al. Retinol binding protein 4 (RBP4) is primarily associated with adipose tissue mass in children. *Int J. Pediatr. Obes.* **6**, e345–e352 (2011).

24. Liu, C. et al. RBP4 Is Associated With Insulin Resistance in Hyperuricemia-Induced Rats and Patients With Hyperuricemia. *Front Endocrinol. (Lausanne)* **12**, 653819 (2021).

25. Duma, N., Santana-Davila, R. & Molina, J. R. Non-Small Cell Lung Cancer: Epidemiology, Screening, Diagnosis, and Treatment. *Mayo Clin. Proc.* **94**, 1623–1640 (2019).

26. Hu, X. et al. Serum levels of retinol-binding protein 4 and the risk of non-small cell lung cancer: A case-control study. *Med. (Baltim.)* **99**, e21254 (2020).

27. Karunanithi, S. et al. RBP4-STRA6 Pathway Drives Cancer Stem Cell Maintenance and Mediates High-Fat Diet-Induced Colon Carcinogenesis. *Stem Cell Rep.* **9**, 438–450 (2017).

28. Baumann, C. A. & Saltiel, A. R. Spatial compartmentalization of signal transduction in insulin action. *Bioessays* **23**, 215–222 (2001).

29. Boucher, J., Kleinridders, A. & Kahn, C. R. Insulin receptor signaling in normal and insulin-resistant states. *Cold Spring Harb. Perspect. Biol.* **6**, a009191 (2014).

30. Poloz, Y. & Stambolic, V. Obesity and cancer, a case for insulin signaling. *Cell Death Dis.* **6**, e2037 (2015).

31. Negrutskii, B. Non-translational Connections of eEF1B in the Cytoplasm and Nucleus of Cancer Cells. *Front Mol. Biosci.* **7**, 56 (2020).

32. Bchini, R., Girardet, J. M., Sormani, R., Gelhaye, E. & Morel-Rouhier, M. Oxidized glutathione promotes association between eukaryotic translation elongation factor 1Bgamma and Ure2p glutathione transferase from Phanerochaete chrysosporium. *FEBS J.* **288**, 2956–2969 (2021).

33. Pisani, C. et al. eEF1Bgamma binds the Che-1 and TP53 gene promoters and their transcripts. *J. Exp. Clin. Cancer Res.* **35**, 146 (2016).

34. Al-Maghrebi, M. et al. The 3' untranslated region of human vimentin mRNA interacts with protein complexes containing eEF-1gamma and HAX-1. *Nucleic Acids Res.* **30**, 5017–5028 (2002).

35. Liu, D. et al. eEF1Bgamma is a positive regulator of NF-small ka, CyrillicB signaling pathway. *Biochem Biophys. Res Commun.* **446**, 523–528 (2014).

36. Yang, Q. et al. Serum retinol binding protein 4 contributes to insulin resistance in obesity and type 2 diabetes. *Nature* **436**, 356–362 (2005).

37. van Dam, R. M. & Hu, F. B. Lipocalins and insulin resistance: etiological role of retinol-binding protein 4 and lipocalin-2?. *Clin. Chem.* **53**, 5–7 (2007).

38. Blaner, W. S., Paik, J., Brun, P. J. & Golczak, M. Retinoids and retinoid-binding proteins: Unexpected roles in metabolic disease. *Curr. Top. Dev. Biol.* **161**, 89–111 (2025).

39. Wlodarczyk, B., Gasiorowska, A., Borkowska, A. & Malecka-Panas, E. Evaluation of insulin-like growth factor (IGF-1) and retinol binding protein (RBP-4) levels in patients with newly diagnosed pancreatic adenocarcinoma (PDAC). *Pancreatology* **17**, 623–628 (2017).

40. Wang, D. D. et al. Preoperative serum retinol-binding protein 4 is associated with the prognosis of patients with hepatocellular carcinoma after curative resection. *J. Cancer Res Clin. Oncol.* **137**, 651–658 (2011).

41. Tang, W., Li, X., Ma, Z. Z. & Li, C. Y. Significance of Retinol-Binding Protein Expression in Patients with Acute Myeloid Leukemia]. *Zhongguo Shi Yan Xue Ye Xue Za Zhi* **26**, 417–421 (2018).

42. Jiao, C., Cui, L., Ma, A., Li, N. & Si, H. Elevated Serum Levels of Retinol-Binding Protein 4 Are Associated with Breast Cancer Risk: A Case-Control Study. *PLoS One* **11**, e0167498 (2016).

43. Wang, Y., Wang, Y. & Zhang, Z. Adipokine RBP4 drives ovarian cancer cell migration. *J. Ovarian Res* **11**, 29 (2018).

44. Papiernik, D. et al. Retinol-Binding Protein 4 Accelerates Metastatic Spread and Increases Impairment of Blood Flow in Mouse Mammary Gland Tumors. *Cancers (Basel)* **12**, 623 (2020).

45. Li, M. et al. Down-regulation of RBP4 indicates a poor prognosis and correlates with immune cell infiltration in hepatocellular carcinoma. *Biosci. Rep.* **41**, BSR20210328 (2021).

46. Park, J. et al. Exoenzyme Tat-C3 inhibits association of zymosan particles, phagocytosis, adhesion, and complement binding in macrophage cells. *Mol. Cells* **16**, 216–223 (2003).

47. Kim, J. G. et al. RhoA GTPase phosphorylated at tyrosine 42 by src kinase binds to beta-catenin and contributes transcriptional regulation of vimentin upon Wnt3A. *Redox Biol.* **40**, 101842 (2021).

48. Fernandez, J., Gharahdaghi, F. & Mische, S. M. Routine identification of proteins from sodium dodecyl sulfate-polyacrylamide gel electrophoresis (SDS-PAGE) gels or polyvinyl difluoride membranes using matrix assisted laser desorption/ionization-time of flight-mass spectrometry (MALDI-TOF-MS). *Electrophoresis* **19**, 1036–1045 (1998).

49. Cap, K. C., Kim, J. G., Hamza, A. & Park, J. B. P-Tyr42 RhoA GTPase amplifies superoxide formation through p47phox, phosphorylated by ROCK. *Biochem Biophys. Res Commun.* **523**, 972–978 (2020).

50. Kim, H. J., Kim, J. G., Moon, M. Y., Park, S. H. & Park, J. B. IkappaB kinase gamma/nuclear factor-kappaB-essential modulator (IKKgamma/NEMO) facilitates RhoA GTPase activation, which, in turn, activates Rho-associated KINASE (ROCK) to phosphorylate IKKbeta in response to transforming growth factor (TGF)-beta1. *J. Biol. Chem.* **289**, 1429–1440 (2014).

Acknowledgements

Author contributions

Competing interests

The authors declare no competing interests.

Ethical approval

The animal study was approved by the Experimental Animal Welfare Ethics Committee, Hallym University (approval number: Hallym2017-3 and 2022-6). We have complied with all relevant ethical regulations for animal testing.

Additional information

Supplementary information The online version contains supplementary material available at https://doi.org/10.1038/s42003-025-08247-w.

Correspondence and requests for materials should be addressed to Jae-Bong Park.

Peer review information *Communications Biology* thanks Sunbin Ling, Jiang Chen, and Da-Liang Ou for their contribution to the peer review of this work. Primary Handling Editors: Georgios Giamas and Johannes Stortz. A peer review file is available.

Reprints and permissions information is available at http://www.nature.com/reprints

Publisher's note Springer Nature remains neutral with regard to jurisdictional claims in published maps and institutional affiliations.